The high frequency limit of spectroscopy

Vladimir U. Nazarov*
Moscow Institute of Physics and Technology (National Research University), Dolgoprudny, Russian Federation

Roi Baer†
Fritz Haber Research Center for Molecular Dynamics and Institute of Chemistry, Hebrew University of Jerusalem, Jerusalem 9190401, Israel

We consider a quantum-mechanical system, finite or extended, initially in its ground-state, exposed to a time-dependent potential pulse, with a slowly varying envelope and a carrier frequency ω_0. By working out a rigorous solution of the time-dependent Schrödinger equation in the high-ω_0 limit, we show that the linear response is completely suppressed after the switch-off of the pulse. We show, at the same time, that to the lowest order in ω_0^{-1}, observables are given in terms of the linear density response function $\chi(\mathbf{r},\mathbf{r}',\omega)$, despite the problem's nonlinearity. We propose a new spectroscopic technique based on these findings, which we name the Nonlinear High-Frequency Pulsed Spectroscopy (NLHFPS). An analysis of the jellium slab and sphere models reveals very high surface sensitivity of NLHFPS, which produces a richer excitation spectrum than accessible within the linear-response regime. Combining the advantages of the extraordinary surface sensitivity, the absence of constraints by the conventional dipole selection rules, and the ease of theoretical interpretation by means of the linear response time-dependent density functional theory, NLHFPS has the potential to evolve into a powerful characterization method in nanoscience and nanotechnology.

In optical spectroscopy, we use light-based probes to study the investigated systems' structure and composition. A significant part of spectroscopy involves linear effects, such as when light is absorbed or scattered off material targets, allowing their imaging and characterization, teaching us almost solely about dipole-allowed transitions. Nonlinear spectroscopy methods go beyond this limitation, studying otherwise hidden or dark transitions applicable to a large variety of systems and processes [1]. Examples of nonlinear spectroscopy include the second-order harmonic generation (SHG) approach, used to study interfaces and adsorbed molecules and serves as high-resolution optical microscopy in biological systems [2], multiphoton excitation fluorescence (MPEF) used for imaging in biological systems, as well as various Raman scattering methods [3]. This paper introduces what can arguably be considered the ultimate nonlinear spectroscopy: a rigorous high-frequency limit of molecular spectroscopy leading to new spectroscopic techniques applicable to molecules and materials. The new spectroscopy relies on the second-order derivatives of the system's nuclear electric potential. As a result, the spectroscopy is sensitive to surfaces and film structure. It can also lead to new types of spectra in molecules.

Nonlinear optical (NLO) methods form a group of powerful experimental techniques for characterizing molecular, biomolecular, condensed matter systems, including materials of reduced dimensionality. The use of nonlinear spectroscopies, especially in surface science and nanoscale systems, is growing due to their high interfacial sensitivity. However, nonlinear spectroscopy is often more challenging to interpret since results may be sensitive to experimental artifacts.

In this paper, we single out a pathway leading to a simplification in nonlinear optical spectroscopy theory based on the observation that, after the end of the pulse acting on the system, the target material's linear-response properties are suppressed for a high carrier frequency. Moreover, we find that the residual excitation, due to the nonlinear processes only, can be expressed in terms of the *linear electron density response function*, the latter occurring on the time-scale of the pulse's enveloping shape. By this, we build an approach to the nonlinear light-matter interaction problem in the case of high-frequency pulses, which turns out no more theoretically and computationally demanding than the solution of the conventional linear response problem. Specifically, the well-developed methods of the linear response time-dependent density functional theory (TDDFT) [4] can be readily invoked, expanding the reach of the latter to the realm of the nonlinear phenomena.

In the proposed approach, applying to high-frequency pulses of arbitrary shapes, we focus on those modulated with the second (low) frequency. The second frequency serves as a natural probe parameter for the nonlinear excitation spectra. We validate the new theory numerically using the exactly solvable hydrogen atom system propagating under a time-dependent field. Then we consider two applications, to nano-films and nano-dots, which demonstrate the power of the proposed method by revealing the modes in the excitation spectra of these systems, latent when probed within the linear response regime.

Formalism.–Within the non-relativistic quantum mechanics, we consider a many-electron system subject to the time-dependent (TD) modulated periodic potential. We are concerned with solving the Schrödinger equation (in the following, we use atomic units unless indicated

* nazarov.vu@mipt.ru
† roi.baer@huji.ac.il

otherwise),

$$i\frac{\partial\Psi(t)}{\partial t} = \left[\hat{H}_0 + \cos\omega_0 t\hat{R}(t)\right]\Psi(t), \tag{1}$$

where the unperturbed Hamiltonian is

$$\hat{H}_0 = \sum_{i=1}^{N}\left[-\frac{1}{2}\nabla_i^2 + v_{ext}(\mathbf{r}_i)\right] + \frac{1}{2}\sum_{i\neq j}^{N}\frac{1}{|\mathbf{r}_i-\mathbf{r}_j|}, \tag{2}$$

N and $v_{ext}(\mathbf{r})$ being the number of electrons and the external (e.g., nuclear Coulomb) potential, respectively, and the harmonic perturbation being enveloped with the potential

$$\hat{R}(t) = \sum_{i=1}^{N} R(\mathbf{r}_i, t). \tag{3}$$

A detailed account of the mathematical development, with very general results, is given in the Appendix A. Here we provide only final results for cases of special interest, for example, when the time-dependence in the pulse potential $R(\mathbf{r},t)$ factorizes, i.e.,

$$R(\mathbf{r},t) = C(t)R(\mathbf{r}), \tag{4}$$

where $C(t)$ is the pulse envelope and $R(\mathbf{r})$ is the potential. It is important to differentiate between two cases, depending on whether $R(\mathbf{r})$ is linear in $\mathbf{r}$ (the *dipole approximation*) or not. In the non-dipole case the probability amplitude for finding the many-body wave function in an excited eigenstate $\Psi_{\alpha\neq 0}$ of energy E_α is, to leading order in ω_0^{-n}, is:

$$\langle\Psi_{\alpha\neq 0}|\tilde{\Psi}(\infty)\rangle = \frac{\pi\widetilde{C^2}(E_\alpha - E_0)}{2i\omega_0^2}\int\langle\Psi_\alpha|\hat{n}(\mathbf{r})|\Psi_0\rangle F_{nd}(\mathbf{r})d\mathbf{r}, \tag{5}$$

where $\hat{n}(\mathbf{r}) = \sum_{i=1}^{N}\delta(\mathbf{r}_i - \mathbf{r})$ is the electron density operator,

$$\widetilde{C^2}(\omega) = \frac{1}{2\pi}\int e^{i\omega t}C^2(t)dt \tag{6}$$

is the pulse envelop frequency-auto-correlation function and

$$F_{nd}(\mathbf{r}) = [\nabla R(\mathbf{r})]^2. \tag{7}$$

Further development then shows, that the time-dependent oscillation in the electron density of the system after the pulse ends are given by

$$\Delta n(\mathbf{r},t) = -\frac{i}{\omega_0^2}\int e^{-i\omega t}\widetilde{C^2}(\omega)\mathrm{Im}\chi(\mathbf{r},\mathbf{r}',\omega)F_{nd}(\mathbf{r}')d\mathbf{r}'d\omega, \tag{8}$$

where $\chi(\mathbf{r},\mathbf{r}',\omega)$ is the density-density response function of the interacting electron system. To leading order in ω_0^{-1} we find the density oscillations proportional to ω_0^{-2} while the total energy absorbed by the system is proportional to ω_0^{-4}, as can be seen in the final expression:

$$\Delta E = -\frac{\pi}{4\omega_0^4}\times \int\omega|\widetilde{C^2}(\omega)|^2 F_{nd}(\mathbf{r})\mathrm{Im}\chi(\mathbf{r},\mathbf{r}',\omega)F_{nd}(\mathbf{r}')d\omega d\mathbf{r}d\mathbf{r}'. \tag{9}$$

In the dipole case

$$R(\mathbf{r}) = -\mathbf{E}\cdot\mathbf{r} \tag{10}$$

equations (5), (8) and (9) are replaced with

$$\langle\Psi_{\alpha\neq 0}|\Psi(\infty)\rangle = \frac{\pi\mathcal{E}_0^2\widetilde{C^2}(E_\alpha - E_0)}{2i\omega_0^4}\int\langle\Psi_\alpha|\hat{n}(\mathbf{r})|\Psi_0\rangle F_d(\mathbf{r})d\mathbf{r}, \tag{11}$$

$$\Delta n(\mathbf{r},t) = -\frac{\mathcal{E}_0^2}{i\omega_0^4}\int e^{-i\omega t}\widetilde{C^2}(\omega)\mathrm{Im}\chi(\mathbf{r},\mathbf{r}',\omega)F_d(\mathbf{r}')d\mathbf{r}'d\omega, \tag{12}$$

and

$$\Delta E = -\frac{\pi\mathcal{E}_0^4}{4\omega_0^8}\times \int\omega|\widetilde{C^2}(\omega)|^2 F_d(\mathbf{r})\mathrm{Im}\chi(\mathbf{r},\mathbf{r}',\omega)F_d(\mathbf{r}')d\omega d\mathbf{r}d\mathbf{r}', \tag{13}$$

where

$$F_d(\mathbf{r}) = [\hat{\boldsymbol{\mathcal{E}}}_0\cdot\nabla]^2 v_{ext}(\mathbf{r}), \tag{14}$$

and $\hat{\boldsymbol{\mathcal{E}}}_0$ is the unit vector along $\boldsymbol{\mathcal{E}}_0$.

Hydrogen atom. We now investigate how the high frequency limit is approached as the frequency increases, by a calculation for an exactly solvable system, namely the hydrogen atom. Assuming the atom is initially in its ground state and subject to the modulated Gaussian pulse

$$C(t) = e^{-t^2/\sigma^2}\cos\omega t \tag{15}$$

and a spherically symmetric quadruple potential

$$R(\mathbf{r},t)\cos\omega_0 t = R_0 r^2 C(t)\cos\omega_0 t, \tag{16}$$

we numerically time-propagate the Scrödinger equation (1). Upon the end of the pulse, we look at the populations of the excited states, plot them in Fig. 1 versus the enveloping function frequency ω (the *second* frequency), and compare with the asymptotic limit. The latter, according to Eqs. (5), (7), and (16) is given by

$$\langle\phi_{ns}|\tilde{\phi}(\infty)\rangle = \frac{2\pi R_0^2}{i\omega_0^2}\widetilde{C^2}(\epsilon_n - \epsilon_1)\langle\phi_{ns}(r)|r^2|\phi_{1s}(r)\rangle, \tag{17}$$

where $\phi_{ns}(r)$ are the hydrogenic s-orbitals and ϵ_n are the corresponding eigenenergies. Similarly, in the dipole

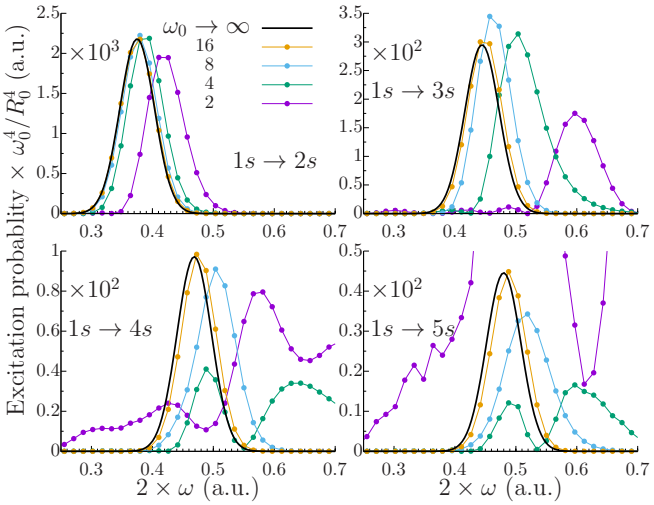

FIG. 1. Excitation probability, upon the end of the pulse of Eq. (16), from the ground-state of the hydrogen atom to its excited states. The black thick line is the asymptotic limit of Eq. (17). Spectra at finite frequencies are obtained by the numerical propagation of the TD Schrödinger equation. The parameters of the pulse used were $\sigma = 50$ a.u. and $R_0 = 0.125$ a.u.

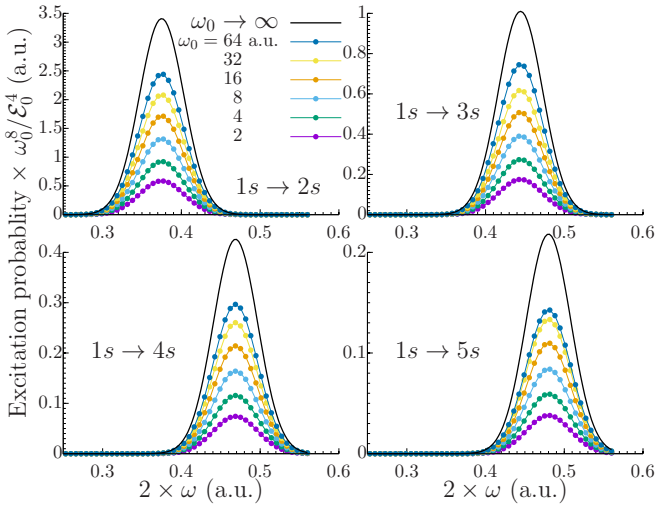

FIG. 2. Excitation probability, upon the end of the pulse of Eq. (18), from the ground-state of the hydrogen atom to its excited s-states. The black thick line is the asymptotic limit of Eq. (20). Spectra at finite frequencies are obtained by the numerical propagation of the TD Schrödinger equation. The parameters of the pulse used were $\sigma = 50$ a.u. and $\mathcal{E}_0 = 0.125$ a.u.

case, we propagate the system under the potential

$$R(\mathbf{r},t)\cos\omega_0 t = -\mathcal{E}_0 z C(t)\cos\omega_0 t. \tag{18}$$

Since $v_{ext}(\mathbf{r}) = -1/r$, for a final state of the s-symmetry we have

$$\langle\phi_{ns}(r)|F_d(\mathbf{r})|\phi_{1s}(r)\rangle = -\frac{1}{3}\langle\phi_{ns}(r)|\left(\nabla^2 1/r\right)|\phi_{1s}(r)\rangle, \tag{19}$$

which, with account of $\nabla^2 1/r = -4\pi\delta(\mathbf{r})$, simplifies Eq. (11) to

$$\langle\phi_{ns}|\tilde{\phi}(\infty)\rangle = \frac{\pi\mathcal{E}_0^2}{6i\omega_0^4}\widetilde{C^2}(\epsilon_n - \epsilon_1)\phi_{ns}(0)\phi_{1s}(0), \tag{20}$$

where $\phi_{ns}(0) = 2/n^{3/2}$ [5].

Figures 1 and 2 demonstrate the convergence, with the growing ω_0, of the excitation processes' outcome to its $\omega_0 \to \infty$ limits of Eqs. (5) and (11), for the cases of the quadruple and dipole exciting fields, respectively. Remarkably, in the quadruple (Fig. 1) and the dipole (Fig. 2) cases the asymptotic regime is approached in very different ways: in the former case the peaks' positions and shape change dramatically with the frequency growth, while in the latter, it is the amplitude of the peaks which changes monotonously only.

It is highly instructive to follow the excitation process in time, from the pulse beginning to its end, in order to see how the system reaches its final state. In Fig. 3, we plot the time-evolution of the population numbers of the $2s$- and $2p$- orbitals of H atom under the action of the pulse of Eq. (18). We observe the principal difference between the change of the occupancies of the s- and p-levels: while the latter gets much more (approximately three orders of magnitude) populated in the middle of the pulse duration, it gives the electron away upon the pulse end, while the former keeps the accepted electron with finite probability. This type of behavior is characteristic for spherically symmetric systems in the high-frequency regime, which is in accordance with our asymptotic theory. This is the linear response that dominates the $s \to p$ transition at the time of the pulse duration, which is gone upon the pulse's extinction. Importantly, we conclude that the usual dipole selection rules do not play a role in this process.

Jellium slab.– We proceed by considering a slab of the thickness d with the positive constant background charge density $n_+ = (\frac{4}{3}\pi r_s^3)^{-1}$, where r_s is the 3D density parameter. Within the Kohn-Sham (KS) density-functional theory (DFT) [6] and using the local density approximation (LDA), we calculate the ground-state KS band structure and electron density. To this system, we apply the doubly modulated dipole pulse of Eqs. (15) and (18), and we use our theory to determine the total energy transfer from the pulse to the slab in the high carrier frequency regime. The problem being one-dimensional, the operator in Eq. (14) reduces to the Laplacian, and we have by virtue of the Poisson law

$$F_d(z) = -4\pi n_+(z) = -4\pi n_+\Theta\left(\frac{d}{2} - |z|\right), \tag{21}$$

where $\Theta(x)$ is the Heaviside's step-function. Resulting absorption spectra, obtained through Eq. (13) with the use of the adiabatic time-dependent LDA (ATDLDA) in the construction of $\chi(\mathbf{r},\mathbf{r}',\omega)$ [4], are presented in Figs. 4

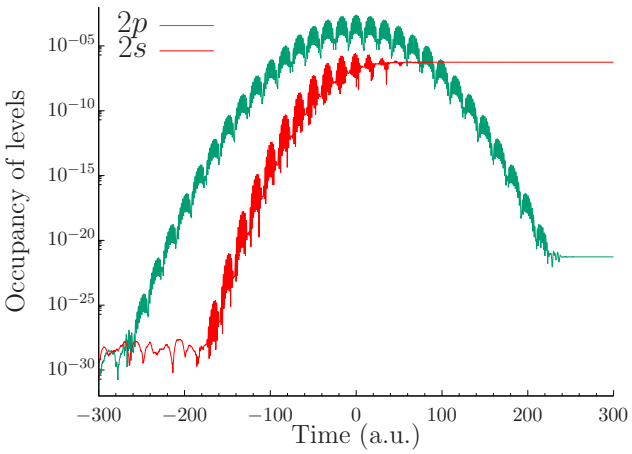

FIG. 3. Evolution of the populations of orbitals in H atom during the action of the pulse of Eq. (18). Parameters used were $\omega_0 = 2$ a.u., $\omega = (\epsilon_2 - \epsilon_1)/2 = 0.1875$ a.u., $\sigma = 50$ a.u., and $\mathcal{E}_0 = 0.125$ a.u.

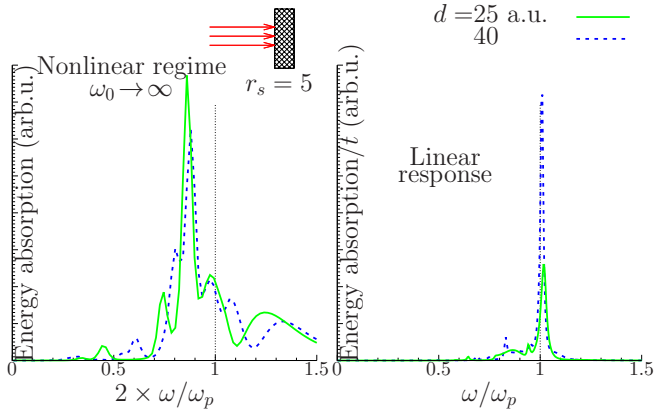

FIG. 4. Jellium slabs. Left: absorption from the pulse of Eqs. (15), (18) ($\sigma = 500$ a.u.) at asymptotically large frequency ω_0 as a function of 2ω, as obtained through Eq. (13). Right: absorption per unit time from the monochromatic field of the frequency ω in the linear response regime. Two slabs of the thicknesses $d = 25$ and 40 a.u. and the density parameter $r_s = 5$ are considered. x-axes are scaled to the bulk plasma energy $\omega_p = 4.2$ eV. Parameters used correspond to the jellium model of solid potassium.

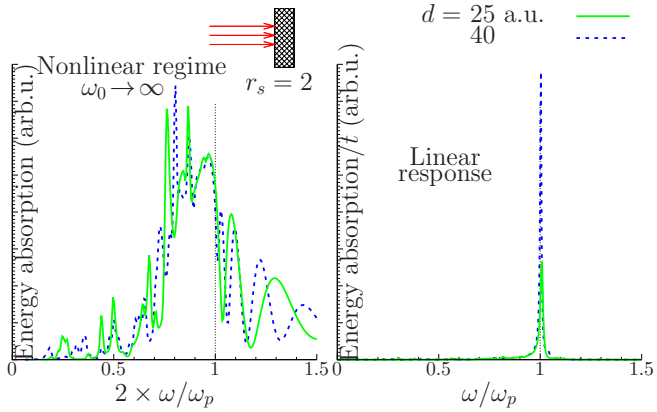

FIG. 5. Same as Fig. 4, but for slabs of the density parameter $r_s = 2$ and the corresponding bulk plasma energy $\omega_p = 16.7$ eV (jellium model of solid aluminum).

and 5, for $r_s = 5$ and 2, corresponding to the jellium model of the metallic potassium and aluminum, respectively. The following observations are made: (i) Similar to the case of the hydrogen atom, due to the integration with $|\widetilde{C^2}(\omega)|^2$ in Eq. (13) and due to the form of the pulse (18), the spectra in the left panels of Figs. 5 and 4, as functions of ω, are governed by the second harmonic generation (SHG) and, accordingly, peaks' positions scale to half the frequencies of the corresponding excitations; (ii) In the linear response regime (right panels in Figs. 4 and 5), spectra are dominated by the bulk plasmon (BP) peak, the intensity of which crucially depends on the share of the bulk, i.e., the slab thickness d. On the contrary, the nonlinear spectra in the high-frequency regime (left panels in Figs. 4 and 5) weakly depend on d, suggesting that they are dominated by the surface excitations. The prevalence of the surface response can be understood by noting that $\int \chi(\mathbf{r}, \mathbf{r}', \omega) d\mathbf{r}' = 0$ (no reaction to a constant potential) and, therefore, both the deep interior and exterior of the slab, by Eq. (21), do not contribute appreciably to the integral of Eq. (13).

Notably, in the left panel of Fig. 4 we observe a strong peak with the maximum at $2\omega \approx 0.88\omega_p$. The counterpart of this peak in the linear response regime (right panel of Fig. 4) is positioned at $\omega \approx 0.83\omega_p$, and it is known as the multipole surface plasmon (MP) [7]. Because of the BP suppression, MP is very prominent in the left panel of this figure, which makes the high-frequency nonlinear technique an ideal tool to study this otherwise subtle type of excitation. It is instructive to note that $F_d(z)$ of Eq. (21) provides, effectively, the *impact* mode of the complementary linear response problem, which is known to be favorable for MP excitation [8]. In Fig. 5 ($r_s = 2$), left panel, we also see a prominent broad peak at 2ω below the BP frequency, while MP is indistinguishable in the linear response spectrum in the right panel. We, therefore, conclude that the corresponding excitation exists at the surface of metallic aluminum, and the high-frequency nonlinear technique provides a unique way to detect it, while the traditional method of the electron energy loss spectroscopy (EELS) does not possess sufficient sensitivity [7]. The oscillating structures at $2\omega > \omega_p$ in Figs. 4 and on both sides from ω_p in Fig. 5 differ for different slab thicknesses, and they can, therefore, be attributed to the interference effect between the two surfaces of the slabs. Finally, the absence of the conventional (dipole) surface plasmon (SP) peak at $\omega_s = \omega_p/\sqrt{2}$ is due to the strictly normal to the surface direction of the exciting field ($q_\parallel = 0$), in which case the amplitude of the SP vanishes.

Jellium sphere.– In contrast to a slab, for a sphere, the

second derivative in the RHS of Eq. (14) does not reduce to Laplacian and, consequently, $F_d(\mathbf{r})$ is not given by the positive background density. Instead, we have

$$F_d(\mathbf{r}) = \frac{2\sqrt{4\pi}n_+}{3}\times \left[\frac{2}{\sqrt{5}}\frac{R^3}{r^3}\Theta(r-R)Y_{20}(\theta,\phi) - \Theta(R-r)Y_{00}(\theta,\phi)\right], \quad (22)$$

where R is the radius of the rigid positive-charge background and $Y_{lm}(\theta,\phi)$ are the spherical functions. Due to the symmetry, the density-response function $\chi(\mathbf{r},\mathbf{r}',\omega)$ splits in angular momentum into $\chi_{lm}(r,r',\omega)$, the latter acting separately on each harmonic of the externally applied potential. The problem becoming one-dimensional again, we calculate χ_{00} and χ_{20}, apply them to Eq. (22), and plug the result into Eq. (13). We consider the same form of the doubly modulated dipole pulse of Eqs. (15), (18) as previously.

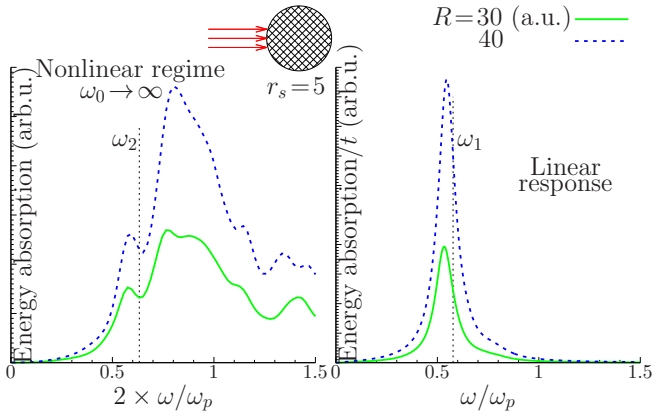

FIG. 6. Jellium spheres. Left: absorption from the pulse of Eqs. (15) – (18) (σ = 500 a.u.) at asymptotically large frequency ω_0 as a function of 2ω, as obtained through Eq. (13). Right: absorption per unit time from the monochromatic field of the frequency ω_0 in the linear response regime. Positions of classical Mie plasmons ω_l are shown by vertical lines. Two spheres of the radii R = 30 and 40 a.u. and the density parameter $r_s = 5$ are considered.

In Fig. 6, results of calculations for two spheres, with radii R = 30 and 40 a.u., and the density parameter $r_s = 5$, are presented, for the nonlinear $\omega_0 \to \infty$ and the linear-response regimes, in the left and right panels, respectively. Within the classical electrodynamics, a sphere of the Drude metal supports an infinite series of Mie plasmons $\omega_l = \sqrt{l/(2l+1)}\omega_p$, $l = 1, 2, \ldots$ [9]. In the monochromatic linear-response (right panel of Fig. 6), we observe the p-mode only of this series, red-shifted by the quantum size effect.

According to Eq. (22), energy absorption in the nonlinear $\omega_0 \to \infty$ regime (left panel of Fig. 6) originates from the superposition of the s- and d-modes. As plotted versus the second modulation frequency ω, it reveals a rich spectrum of the underlying excitations. The leftmost feature near $0.57\omega_p$ comes from the d-mode Mie plasmon ω_2, red-shifted in the quantum calculation. The dominating broad peak with the maximum near $0.80\omega_p$ does not have an analogue within the classical electrodynamics, and, similar to the multipole plasmon modes in the case of a slab, it is made accessible with the use of the high-ω_0 nonlinear regime. A signature of the bulk plasmon on the right shoulder of this peak can be also observed, indicating the possibility of the direct recognition of the constituents of nano-particles by their bulk plasmon frequencies ω_p with the use of laser pulses. The latter is, obviously, impossible in the linear-response regime. We also note structures above ω_p, which are due to the (dressed) single-particle excitations, affected by the quantum interference.

In conclusions, we have considered the excitation of an arbitrary quantum-mechanical system by an externally applied electric field of high frequency ω_0 and finite duration. After the end of the pulse, the state of the system being a superposition of the eigenstates of the unperturbed Hamiltonian, the expansion of the corresponding transition amplitudes in the power series in ω_0^{-1} has been performed, with the leading terms found of the order ω_0^{-4} for the uniform applied field (dipole case) and of ω_0^{-2}, otherwise.

We have demonstrated that, to the leading order in the inverse frequency, the quadratic, rather than the linear, response determines the excitation process. Nonetheless, we have shown that all the information necessary to describe this nonlinear excitation regime is contained in the linear density response function of the system under consideration. The problem has been thus reduced to that of the linear response time-dependent density functional theory, for which effective methods of solution, at various levels of accuracy and sophistication, are well established.

We have, further, found that a specific pulse shape, that with the modulation by the second (low) frequency, can be particularly useful as a probe, delivering spectra of excitations in the nonlinear response regime. In our illustrative applications, to the jellium model nano-films and nano-dots, plasmonic modes undetectable or difficult for the detection by the linear optical spectroscopy or electron energy-loss spectroscopy, have been clearly discerned. We point out that the high carrier frequency is out of resonance, and its only role is to set the scene for probing the system with the second frequency, the twice of the latter being in resonance with the system's excitations.

Our results evidence that the excitation by the finite-duration field of high frequency, modulated with another frequency, being *per se* an interesting phenomenon rich with profound physics, can serve, at the same time, as an efficient nonlinear spectroscopic method to probe the modes inaccessible or hardly accessible by other techniques. The decisive advantage of the proposed method, which can be tentatively named the Nonlinear High-Frequency Pulsed Spectroscopy, is its clear-cut underlying theoretical basis of the linear response TDDFT. By this, the comparison between experiment and theory is

greatly facilitated, opening exciting new opportunities in the field of the light-matter interactions.

ACKNOWLEDGMENTS

V.U.N. acknowledges the hospitality of the Fritz Haber Center for Molecular Dynamics and Institute of Chemistry, Hebrew University of Jerusalem.

[1] S. Mukamel, *Principles of Nonlinear Optical Spectroscopy* (Oxford University Press, New York, 1995).

[2] S. Roke and G. Gonella, Nonlinear Light Scattering and Spectroscopy of Particles and Droplets in Liquids, Annual Review of Physical Chemistry **63**, 353 (2012).

[3] P. K. Johansson, L. Schmüser, and D. G. Castner, Nonlinear Optical Methods for Characterization of Molecular Structure and Surface Chemistry, Topics in Catalysis **61**, 1101 (2018).

[4] E. K. U. Gross and W. Kohn, Local density-functional theory of frequency-dependent linear response, Phys. Rev. Lett. **55**, 2850 (1985).

[5] L. D. Landau and E. M. Lifshitz, *Quantum Mechanics: The Non-Relativistic Theory* (Butterworth-Heinemann, London, 1981).

[6] W. Kohn and L. J. Sham, Self-consistent equations including exchange and correlation effects, Phys. Rev. **140**, A1133 (1965).

[7] K.-D. Tsuei, E. W. Plummer, A. Liebsch, K. Kempa, and P. Bakshi, Multipole plasmon modes at a metal surface, Phys. Rev. Lett. **64**, 44 (1990).

[8] V. U. Nazarov, Multipole surface-plasmon-excitation enhancement in metals, Phys. Rev. B **59**, 9866 (1999).

[9] C. F. Bohren and D. R. Huffman, *Absorption and Scattering of Light by Small Particles* (John Wiley & Sons, Inc., New York, 1998).

Appendix A: Details of derivations

In the interaction representation

$$\tilde{\Psi}(t) = e^{i\hat{H}_0 t}\Psi(t), \tag{A1}$$

$$\tilde{\hat{R}}(t) = e^{i\hat{H}_0 t}\hat{R}(t)e^{-i\hat{H}_0 t}, \tag{A2}$$

the problem of the solution of Eq. (1) turns into that of the solution of the integral equation

$$\tilde{\Psi}(t) = \Psi_0 + \frac{1}{i}\int\limits_{-\infty}^{t} \cos\omega_0 t' \tilde{\hat{R}}(t')\tilde{\Psi}(t')dt', \tag{A3}$$

where Ψ_α is the set of eigenfunctions of the Hamiltonian (2), and we assume that $R(\mathbf{r}, -\infty) = 0$ and the system is initially in its ground-state Ψ_0.

Performing several consecutive integrations by parts in Eq. (A3), assuming the pulse to be of finite duration $[\hat{R}(\mathbf{r}, +\infty) = 0]$ and ω_0 to be large, we obtain, after keeping the terms up to ω_0^{-4} only,

$$\tilde{\Psi}(\infty) = \Psi_0 + \frac{1}{4\omega_0^2}\int\limits_{-\infty}^{\infty}\left[\frac{\partial\tilde{\hat{R}}(t)}{\partial t}, \tilde{\hat{R}}(t)\right]\Psi_0 dt - \frac{1}{4\omega_0^4}\int\limits_{-\infty}^{\infty}\left[\frac{\partial^3\tilde{\hat{R}}(t)}{\partial t^3}, \tilde{\hat{R}}(t)\right]\Psi_0 dt +$$
$$\frac{1}{16\omega_0^4}\int\limits_{-\infty}^{\infty}\left[\frac{\partial\tilde{\hat{R}}(t)}{\partial t}, \tilde{\hat{R}}(t)\right]\int\limits_{-\infty}^{t}\left[\frac{\partial\tilde{\hat{R}}(t')}{\partial t'}, \tilde{\hat{R}}(t')\right]\Psi_0 dt' dt - \frac{1}{16\omega_0^4}\int\limits_{-\infty}^{\infty}\left[\frac{\partial\tilde{\hat{R}}(t)}{\partial t}, \tilde{\hat{R}}^3(t)\right]\Psi_0 dt + \frac{3}{64\omega_0^4}\int\limits_{-\infty}^{\infty}\left[\frac{\partial\tilde{\hat{R}}^2(t)}{\partial t}, \tilde{\hat{R}}^2(t)\right]\Psi_0 dt. \tag{A4}$$

The commutators in Eq. (A4) can be expanded as

$$\left[\frac{\partial\tilde{\hat{R}}(t)}{\partial t}, \tilde{\hat{R}}(t)\right] = ie^{i\hat{H}_0 t}\left[\left[\hat{H}_0, \hat{R}(t)\right], \hat{R}(t)\right]e^{-i\hat{H}_0 t}, \tag{A5}$$

$$\left[\frac{\partial^3\tilde{\hat{R}}(t)}{\partial t^3}, \tilde{\hat{R}}(t)\right] = e^{i\hat{H}_0 t}\left[-i\left[\hat{H}_0, \left[\hat{H}_0, \left[\hat{H}_0, \hat{R}(t)\right]\right]\right] - 3\left[\hat{H}_0, \left[\hat{H}_0, \frac{\partial\hat{R}(t)}{\partial t}\right]\right] + 3i\left[\hat{H}_0, \frac{\partial^2\hat{R}(t)}{\partial t^2}\right], \hat{R}(t)\right]e^{-i\hat{H}_0 t}, \tag{A6}$$

$$\left[\frac{\partial\tilde{\hat{R}}(t)}{\partial t}, \tilde{\hat{R}}^3(t)\right] = ie^{i\hat{H}_0 t}\left[\left[\hat{H}_0, \hat{R}(t)\right], \hat{R}^3(t)\right]e^{-i\hat{H}_0 t}, \tag{A7}$$

$$\left[\frac{\partial\tilde{\hat{R}}^2(t)}{\partial t}, \tilde{\hat{R}}^2(t)\right] = ie^{i\hat{H}_0 t}\left[\left[\hat{H}_0, \hat{R}^2(t)\right], \hat{R}^2(t)\right]e^{-i\hat{H}_0 t}. \tag{A8}$$

Non-dipole case.– We evaluate the commutator (A5) to

$$\left[\left[\hat{H}_0, \hat{R}(t)\right], \hat{R}(t)\right] = -\int [\nabla R(\mathbf{r},t)]^2 \hat{n}(\mathbf{r}) d\mathbf{r}, \tag{A9}$$

If the right-hand side of Eq. (A9) is not zero, then the substitution of Eq. (A9) into Eq. (A4) with keeping only the leading term of the order ω_0^{-2} yields

$$\langle \Psi_{\alpha\neq 0}|\tilde{\Psi}(\infty)\rangle = \frac{1}{4i\omega_0^2}\times \int e^{i(E_\alpha - E_0)t}\langle \Psi_\alpha|\hat{n}(\mathbf{r})|\Psi_0\rangle [\nabla R(\mathbf{r},t)]^2 d\mathbf{r}dt. \tag{A10}$$

If, furthermore, the factorization of Eq. (4) holds then we arrive at Eq. (5).

Using Eq. (5) together with the spectral representation of the many-body interacting density response function

$$\chi(\mathbf{r},\mathbf{r}',\omega) = \sum_{\alpha\neq 0}\left[\frac{\langle\Psi_\alpha|\hat{n}(\mathbf{r}')|\Psi_0\rangle\langle\Psi_0|\hat{n}(\mathbf{r})|\Psi_\alpha\rangle}{E_0 - E_\alpha + \omega + i\eta} + \frac{\langle\Psi_\alpha|\hat{n}(\mathbf{r})|\Psi_0\rangle\langle\Psi_0|\hat{n}(\mathbf{r}')|\Psi_\alpha\rangle}{E_0 - E_\alpha - \omega - i\eta}\right], \tag{A11}$$

where η is a positive infinitesimal, we obtain Eq. (8) for the density oscillations in the system upon the end of the pulse.

For the *total energy* absorbed by the system from the pulse we can write

$$\Delta E = \sum_\alpha E_\alpha |\langle\Psi_\alpha|\tilde{\Psi}(\infty)\rangle|^2 - E_0, \tag{A12}$$

which, with the use of the completeness of the basis set $\sum_\alpha |\langle\Psi_\alpha|\tilde{\Psi}(\infty)\rangle|^2 = 1$, can be rewritten as

$$\Delta E = \sum_{\alpha\neq 0}(E_\alpha - E_0)|\langle\Psi_\alpha|\tilde{\Psi}(\infty)\rangle|^2, \tag{A13}$$

and then, by Eqs. (5) and (A11), finally written in the form of Eq. (9).

Dipole case.– If

$$R(\mathbf{r},t) = -\boldsymbol{\mathcal{E}}(t)\cdot\mathbf{r}, \tag{A14}$$

where $\boldsymbol{\mathcal{E}}(t)$ is the uniform in space electric field, then $[\nabla R(\mathbf{r},t)]^2 = \boldsymbol{\mathcal{E}}^2(t)$, and Eq. (A10) integrates to zero identically. With the use of Eqs. (A4), (A6), and the commutator relations

$$[\hat{H}_0, \sum_{i=1}^N \boldsymbol{\mathcal{E}}\cdot\mathbf{r}_i] = -\sum_{i=1}^N \boldsymbol{\mathcal{E}}\cdot\nabla_i, \tag{A15}$$

$$[\hat{H}_0, [\hat{H}_0, \sum_{i=1}^N \boldsymbol{\mathcal{E}}\cdot\mathbf{r}_i]] = \sum_{i=1}^N \boldsymbol{\mathcal{E}}\cdot\nabla_i v_{ext}(\mathbf{r}_i), \tag{A16}$$

$$[\hat{H}_0, [\hat{H}_0, [\hat{H}_0, \sum_{i=1}^N \boldsymbol{\mathcal{E}}\cdot\mathbf{r}_i]]] = -\sum_{i=1}^N\left\{\frac{1}{2}\boldsymbol{\mathcal{E}}\cdot\nabla_i^3 v_{ext}(\mathbf{r}_i) + [\nabla_i(\boldsymbol{\mathcal{E}}\cdot\nabla_i v_{ext}(\mathbf{r}_i))]\cdot\nabla_i\right\}, \tag{A17}$$

$$[[\hat{H}_0, [\hat{H}_0, [\hat{H}_0, \boldsymbol{\mathcal{E}}\cdot\mathbf{r}]]], \sum_{i=1}^N \boldsymbol{\mathcal{E}}\cdot\mathbf{r}_i] = -\sum_{i=1}^N (\boldsymbol{\mathcal{E}}\cdot\nabla_i)^2 v_{ext}(\mathbf{r}_i), \tag{A18}$$

and noting that in Eq. (A4) the sum of the 4th, 5th, and 6th terms on the RHS evaluates to zero, as it can be directly verified, we arrive at the dipole counterpart of Eq. (A10)

$$\langle\tilde{\Psi}_{\alpha\neq 0}|\Psi(\infty)\rangle = \frac{1}{4i\omega_0^4}\times \int d\mathbf{r}dt e^{i(E_\alpha - E_0)t}\langle\Psi_\alpha|\hat{n}(\mathbf{r})|\Psi_0\rangle[\boldsymbol{\mathcal{E}}(t)\cdot\nabla]^2 v_{ext}(\mathbf{r}). \tag{A19}$$

For the linearly polarized field

$$\boldsymbol{\mathcal{E}}(t) = C(t)\boldsymbol{\mathcal{E}}_0, \tag{A20}$$

we then immediately obtain Eqs. (11)-(13).